Electronic Supplementary Information (ESI)

Chemical Mechanism of the High Solubility Pathway for the Carbon Dioxide Free Production of Iron (Chemical Communications)

Stuart Licht,[*,a] Hongjun Wu,[a] Zhonghai Zhang,[a] Hina Ayub[a]
[a]Department of Chemistry/Solar Institute, George Washington University, Washington, DC 20052, USA.
*CORRESPONDING AUTHOR EMAIL ADDRESS: slicht@gwu.edu

Content

Expanded experimental and thermochemical calculation details

$LiFeO_2$ can be formed from Fe_2O_3 and Li_2CO_3 at < 400°C as measured by x-ray diffraction, XRD from the ball milled reactants.[ESI-1] Another also salt forms spontaneously from lithiated hematite, Fe_2O_3. The ferrospinel $LiFe_5O_8$ was first reported by Hoffman who prepared the compound and measured its XRD.[ESI-2] MFe_5O_8 preparation: At lower reaction temperatures pure $LiFe_5O_8$, size controlled (9-900 nm), has been prepared by sol gel/calcine synthesis or via hydrothermal ball milling.[ESI-3-5] Here, the penta-iron octa-oxides are prepared by ball milling of an equivalent ratio of 5 parts Fe_2O_3 (Baker, 98%) to 1 part of the alkali carbonate (Alfa Aesar 99% Li_2CO_3 or BDH 99.5% Na_2CO_3) for 2 hours at 500 rpm in a Retsch PM100 planetary ball mill, in stainless media, followed by sintering at 800°C for 2 hours. Ball mill of the Fe_2O_3: alkali carbonate 5:1 equivalent mix, prior to heating leads to complete reaction as measured by mass loss of 1 equivalent of CO_2.

Determination of solubility in the molten carbonate Low melting points of carbonates are achieved through a eutectic mix of alkali carbonates (T_{mp} Li_2CO_3: 723°C, Na_2CO_3: 851°C, K_2CO_3: 891°C; $Li_{1.07}Na_{0.93}CO_3$: 499°C; $Li_{0.85}Na_{0.61}K_{0.54}CO_3$: 393°C[ESI-6,7]): Solubility is determined from multiple measurements including compositions, both approaching saturation, and also in compositions containing excess ferric oxide salts. When these salts are in excess in the molten mix, it is observed to descend to the bottom of the molten mix, and is not removed with the molten liquid. The molten liquid is removed from the molten mix and analyzed. The extracted liquid is cooled, ground and mixed with water. The carbonate component is water soluble, while the alkali iron oxide component is not, and is removed by filtration and dried at 100°C to determine the mass fraction of the ferric oxide salt that dissolved in the molten carbonate.

In molten Li_2CO_3 containing dissolved Fe(III), we observe that iron is readily deposited on the cathode with applied potentials as described in Figure 3. Electrolysis cell bodies are straight wall 20 ml nickel crucible (VWR), protected from air oxidation by argon. The anode is the internal cell wall, which when filled with ~15 ml of electrolyte, has a surface area of 30 cm^2, and comprises a cylinder which surrounds an 0.5 cm^2 area, coiled, 1.5 mm diameter iron wire cathode. As noted in Figure 3, in one experiment a 30 cm^2 flat platinum sheet, rolled into a cylinder is used in lieu of the nickel anode, and an alumina crucible is used in lieu of the nickel crucible. In this study the full cell electrolysis potential is measured using the oversized anode to focus on cathode (iron reduction electrode) effects. We have also reported initial anode results[2],

and other anode effects will be the focus of a future study. The electrolysis potential, as a function of concentration, temperature and current density is presented in Figure 3.

Hy-STEP iron production apparatus: In this demonstration a 31.5”x44.5” Fresnel lens (Edmund Optics) concentrates sunlight to provide temperatures of over 950°C, and a Sunforce-44444 400 W wind turbine provides electronic charge, charging series nickel metal hydride, MH, cells at 1.5V). Each MH cell, provides a constant discharge potential of 1.0-1.3 V, which are each used to drive the one or two, series connected iron electrolysis cells as indicated in the Figure 4. The electrolysis cells produce iron at 950°C in lithium carbonate electrolyte containing 14 molal Fe(III), added as Fe_2O_3, and Li_2O.

Electrolysis potentials in Figure 2 are calculated from the thermochemical data (only at unit activity) reported for Fe, Fe_2O_3, $LiFe_5O_8$, Li_2O, Li_2CO_3, CO_2, CO, and O_2.[9,10] As noted in equation 4, other than unit activity coefficients can prevail in various concentrated electrolytes.[ESI-15] Alternatively ion association effects can decrease activity coefficients. High Fe(III) activity coefficients, $\alpha_{Fe(III)} > 1$, would further decrease the thermodynamic potential to produce iron.

It is interesting to note that the observed electrolysis potential at low current density is considerably smaller than the expected thermodynamic potential of 0.8V at 950°C. This is, at least in part, explained by the high, non-unit activity of the dissolved iron (14 m) providing significant voltage and energy savings. While a nickel anode appears stable during extended electrolyses, it is thermodynamically unstable. We have already reported initial anode results[2], and other anode effects will be the focus of a future study, and we note in the rights side of Figure 3, that when the nickel anode is replaced by a platinum electrode there is an observed increased in the measured electrolysis potentials, particularly at high current density.

The chemistry of $LiFeO_2$ and $LiFe_5O_8$

The corrosion product of iron containing alloys in lithium containing eutectic molten carbonates at 650°C is $LiFeO_2$. Of significance, this oxide had been reported as highly insoluble, with a solubility on the order of parts per million.[6] That is beneficial for molten carbonate fuel cells, MCFC’s, electrode stability and has been the basis for a number of $LiFeO_2$ coatings or bulk material for MCFC electrodes.[ESI-8-10] However, that insolubility of $LiFeO_2$ in Li_2CO_3 would not provide a basis for iron production by electrolysis of dissolved iron oxide salts. Collongues and Chaudron concluded that $LiFeO_2$ and $LiFe_5O_8$ are the limiting members of the solid solutions formed by the replacement of $2Fe^{2+}$ by Li^+Fe^{3+} in 2FeO or $2Fe_3O_4$, respectively.[ESI-11]

The synthesis of solid $LiFe_5O_8$ from the complete reaction of a 5:1 mole ratio of powdered Fe_2O_3 and Li_2CO_3, or 10:1 ratio of $Fe(NO_3)_2$ and Li_2CO_3, occurs at elevated temperature and is accelerated under microwave irradiation,[ESI-1,12] and $LiFe_5O_8$ remains stable up to 1000°C,[ESI-13] although on heating it has been reported that lithium ions in the solid state $LiFe_5O_8$ lattice become disordered at temperatures above 755°C, and return to an ordered lattice state the system is cooled at 735°C.[ESI-14]

The chemistry of the CO_2/Li_2O equilibrium in Li_2CO_3

Experimentally, we observe the facile reaction of CO_2 and Li_2O in molten Li_2CO_3. Here, thermodynamically, we also determine the equilibrium conditions between the CO_2, Li_2O and Li_2CO_3 species in the system:

$$Li_2CO_3 \rightleftharpoons Li_2O + CO_2 \qquad (1)$$

Using the known thermochemistry of Li_2O, CO_2 and Li_2CO_3,[10] we calculate the reaction free-energy of equation 1, and from this calculate the thermodynamic equilibrium constant as a function of temperature. From this equilibrium constant, the area above the curve in Figure ESI-1 presents the thermodynamic wide domain in which Li_2CO_3 dominates, that is where excess CO_2 reacts with Li_2O such that $p_{CO2} \bullet a_{Li2O} <$

a_{Li2CO3}. This is experimentally verified in the measured thermogravimetric analysis of Li_2CO_3, Figure ESI-2, and when we dissolve Li_2O in molten Li_2CO_3, and inject CO_2(gas). Through the measured mass gain, we observe the rapid reaction to Li_2CO_3. Hence, CO_2 is flowed into a solution of 5% by weight Li_2O in molten Li_2CO_3 at 750°C, the rate of mass gain is only limited by the flow rate of CO_2 into the cell (using an Omega FMA 5508 mass flow controller) to react one equivalent of CO_2 per dissolved Li_2O. As seen in the thermogrametric analysis in Figure ESI-2, the mass loss in time of heated lithium carbonate heated in an open atmoshphere (~0.03% CO_2) is slow up to 850°C, but accelerates at 950°C. However the mass loss falls to nearly zero, when heated under pure (1 atm) CO_2. Also in accord with Eq. 1 added Li_2O shifts the equlibrium to the left and inbits carbonate decomposition. As seen in the figure in the open atmosphere, molten 100% Li_2CO_3 at 850°C loses mass, while a mixture of 90% by weight Li_2CO_3 and 10% Li_2O exhibits little mass loss in time.

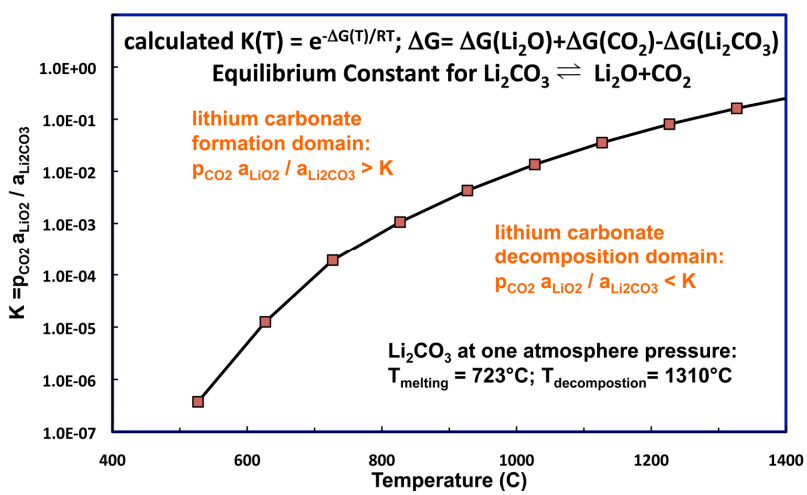

Figure ESI-1. Species stability in the lithium carbonate, lithium oxide, carbon dioxide system as calculated from the thermochemical data for Li_2CO_3, Li_2O, and CO_2.[10]

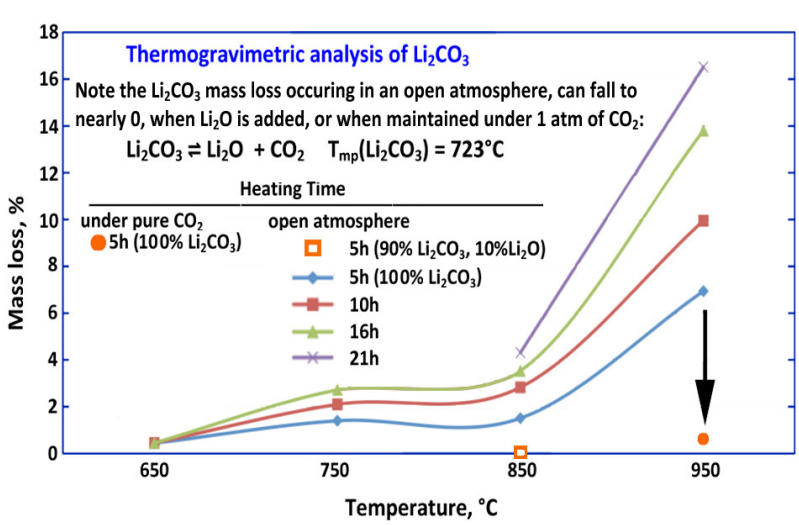

Figure ESI-2. Thermogravimetric analysis of lithium carbonate. The measured mass loss in time of Li_2CO_3.

The chemistry of $LiFeO_2$ and $LiFe_5O_8$ in Li_2CO_3

$LiFe_5O_8$ dissolves rapidly in molten Li_2CO_3, however it reacts with the molten carbonate as evident in the mass loss of the solution. Similarly, Fe_2O_3, reacts with molten Li_2CO_3 resulting in a mass loss due to the evolution of CO_2 proportional to the quantity of Fe_2O_3 contained in the Li_2CO_3 mix. As seen in Fig. ESI-3, over a wide range of temperature and mass fractions of Fe_2O_3 in Li_2CO_3, the system process to release one equivalent of CO_2 for each equivalent of Fe_2O_3, to form a steady state concentration of $LiFeO_2$ in accord with:

$$Fe_2O_3 + Li_2CO_3 \rightarrow 2LiFeO_2 + CO_2 \qquad (2)$$

Alternatively, the dissolution of 1 equivalent of Li_2O and 1 equivalent of Fe_2O_3 in molten Li_2CO_3 can drive the direct dissolution of $LiFeO_2$ mole without the reactive formation of CO_2 in accord with:

$$Fe_2O_3 + Li_2O \rightarrow 2LiFeO_2 \qquad (3)$$

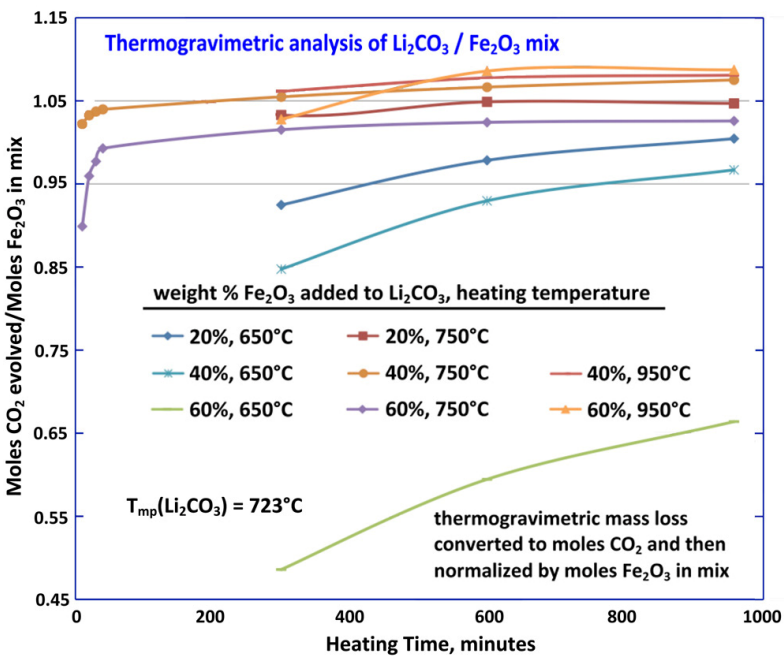

Figure ESI-3. Thermogravimetric analysis of a mix of lithium carbonate with ferric oxide. The measured mass loss in time of Li_2CO_3. As indicated in the figure legend, the mixture is composed of either 20, 40 or 60 weight percent of Fe_2O_3 in Li_2CO_3. The mass loss over time is measured at the indicated constant temperature of either 650, 750 or 950°C, and corrected for CO_2 evolution measured from the 100% Li_2CO_3 melt, then converted to moles of CO_2, and finally normalized by the moles of Fe_2O_3 in the lithium carbonate ferric oxide mix.

Eq. 3 is of particular significance to the electrolysis of Fe_2O_3 in molten carbonate. As $LiFeO_2$ is reduced to iron metal, Li_2O is released ($2LiFeO_2 \rightarrow 2Fe + Li_2O$) facilitating the continued addition and dissolution Fe_2O_3 without CO_2 release, and without a change in the electrolyte. As indicated in Fig. ESI-2, a molar excess, of greater than 1:1 of Li_2O to Fe_2O_3 in molten Li_2CO_3, will further inhibit the Eq. 1 disproportionation of lithium carbonate.

Description of STEP energy conversion

Previously, we demonstrated a solar, carbon dioxide-free process for the production of iron, the STEP (Solar Thermal Electrochemical Photo) iron process[2]. In that process, solar energy is split into IR (thermal) and visible bands, to respectively provide heat and electronic energy to drive the iron electrolysis. **Hy-STEP,** hybrid Solar

Thermal Electrochemical Production provides a synergy of renewable energy driven charge transfer, solar thermal, and electrolysis processes, by applying sunlight to heat a class of (endothermic) reactions, which require less energy at higher temperature. An energy diagram is presented in Figure ESI-4, which compares an energetically forbidden process at room temperature to a generalized energetically permitted STEP or hy-STEP process. Our first experimental example of a STEP process was driving water splitting, which is a 1.2V process at room temperature, which was instead driven by a single small band-gap (1.1V Si) semiconductor, at low potential at high temperature in a molten hydroxide electrolyte.[ESI-16,-18]. Our previous demonstrations of STEP consisted of solar, rather the new wind-solar, hy-STEP process, which replaces solar with wind driven electronic charge transfer. The basis for improved efficiencies using the STEP or hy-STEP process is:

(i) The energy to drive many reactions to decrease greenhouse emissions, such as water splitting to generate hydrogen fuel, CO_2 splitting for carbon capture, or metal oxide reduction to form useful metals, is excessive at room temperature.

(ii) concentrated solar thermal energy can be used to increase the temperature of endothermic electrolysis processes. The electrolysis potential is lowered at higher temperature, substantially improving system efficiency.

Expanded theoretical details of the STEP process are given in reference 3, and expanded experimental details are given in references 2 and 5. This communication focuses on novel aspects of the iron electrolysis cell, while the remaining wind[ESI-19] (electric) and solar thermal (to T > 1000°C) components of Hy-STEP iron are mature technologies. An array of flat mirrors reflecting to a central tower, such as demonstrated by Brightsource can achieve temperatures of 550°C;[ESI-20] individual parabolic heliostat can achieve temperatures over 800°C; [ESI-21] short focal length, plastic fresnel generating optical concentrations of 500-1000 suns have been deployed for concentrator photovoltaics, such as demonstrated by Amonix,[ESI-22] while better mirrors and secondary optics, can achieve temperatures over 1000°C.[ESI-23]

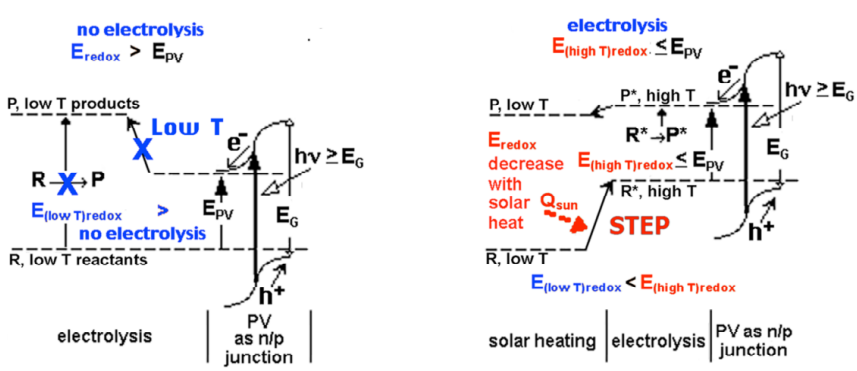

Figure ESI-4. The complete solar spectra drives electrolysis in the **STEP** process. Redirected solar thermal (Q_{sun}) heats incoming reactants to reduce the energy for an electrolysis, which is driven by visible light (hν) PV charge transfer. As one example, the energy of photodriven charge transfer is insufficient (left) to drive (unheated) electrolysis, but is sufficient (right) to drive endothermic in the solar heated STEP process.

Author Contributions. S. L. designed the Hy-STEP process, and together with H. W. and Z. Z conducted the solublity, electrochemical and Hy-STEP measurements analyses. H A. helped S. L. with the iron oxide and CO_2 thermodynamic calculations in the Fig. ESI-1.

Electronic Supplementary Information References

note: numbered references in the ESI text denoted as "x" rather than "ESI-x" refer to references listed in the Chem. Comm. text.

ESI-1. V. Berbenni, A. Marini, A., Capsoni, D. Solid State Reaction Study of the System Li_2CO_3/Fe_2O_3. *Zeitschrift Fur Naturforschung Section A-A J. Phys. Sci*., 1998, **12**, 997-1003.

ESI-2. A. Hoffman, Crystal Chemistry of Lithium Ferrites. *Naturewiss* **26**, 431 (1938).

ESI-3. H. Widatallah, C. Johnson, F. Berry, The influence of ball milling and subsequent calcinations on the formation of $LiFeO_2$. *J. Mat. Sci*. **21**, 4621-4625 (2002)..

ESI-4. H. Yang, Z. Wang, L. Song, M. Zhhao, J. Wang, H. Luo, A study of the coecervity and the magnetic anisotropy of the lithium ferrite nanocrystallite. *J. Phys. D. Appl. Phys*., 1996, ***29***, 2575-2578.

ESI-5. A. Ahniyaz, T. Fujiwara, S. Song, M. Yoshimura, Low temperature preparation of β- $LiFe_5O_8$ fine particles by hydrothermal ball milling. *Sol. State Ionics*, 2002, **151**, 419-423.

ESI-6. E. J. Cairns, D. I. MacDonald, Sensitive Thermal Analysis Establishing Formation of the Incongruently Melting Compound $LiNaCO_3$, *Nature*, 1962, **194**, 441-442.

ESI-7. M. Rolin, Thermodynamic Properties of the alkali metal carbonates. I; The ternary diagram Na_2CO_3-K_2CO_3-Li_2CO_3, *Bull, Soc. Chim. Fr*., 1964, 2104-210.

ESI-8. K. Matsumoto, K. Yuasa, K.,Nakagawa, Protection against localized corrosion of stainless steel below 843 K in molten lithium-sodium carbonate. *Electrochemistry*, 1999, **3**, 253-258.

ESI-9. Li, F., Chen, H., Wang, C., Hu, K. A novel modified NiO cathode for molten carbonate fuel cells. *J. Electroanal. Chem.*, 2002, **1**, 53-60.

ESI-10. A. Wijayasinghe, B. Bergman, C. Lagergren, Cathodes for Molten Carbonate Fuel Cells, *J. Electrochem. Soc.*, 2003, **150**, A558-A564.

ESI-11. R. Collongues, G. Chaudron, Sur la preparation des Ferrites de Lithium, *Compt. Rend*., 1950, **124**, 143-145.

ESI-12. V. Vanetsev, V. Ivanov, Y. Tret'yakov, Microwave Synthesis of Lithium, Copper, Cobalt, and Nickel Ferrites. *Doklady Chem.*, 2002, **387**, 332-334.

ESI-13. N. Zakharchenko, Fe_2O_3-Li_2O Catalysts for Ammonia Oxidation. *Russ. J. Appl. Chem*. 2001, *74*, 229-234.

ESI-14. P. B. A. Braun, A superstructure in spinels, *Nature*, 1952, **170**, 1123.

ESI-15. S. Licht, pH Measurement in concentrated alkaline solution. *Anal. Chem*., 1985, **57**, 514-519.

ESI-16. S. Licht, L. Halperin, M. Kalina, M. Zidman, N. Halperin, Thermochemical Solar Hydrogen Generation*, Chem. Comm.* **2003**, *2003*, 3006-3007.

ESI-17. S. Licht, Electrochemical Potential Tuned Solar Water Splitting, *Chem. Comm.* **2005**, *2005*, 4623-4646.

ESI-18. S. Licht, S. "Solar thermal & solar thermal hybrid generation of hydrogen,"
Chapter 21 in Monograph: *Solar Hydrogen and Nanotechnology,* Wiley, 641-664, 2010.

ESI-19. E. Barbier, How is the global green deal going? *Nature*, 2010, **464**, 832-833.

ESI-20. Power tower solar technologies are described at: brightsourceenergy.com; ausra.com, esolar.com.

ESI-21. Parabolic solar concentrator technologies are described at: stirlingenergy.com.

ESI-22. Fresnel solar concentrator technologies are described at: amonix.com, energy innovations.com/sunflower.

ESI-23. R. Pitz-Paal, High Temperature Solar Concentrators, in *Solar Energy Conversion and Photoenergy Systems*, Eds. Galvez, J. B.; Rodriguez, S. M. **2007**, *EOLSS* Publishers, Oxford, UK.